7-10-2008

Stable Long-Time Semiclassical Description of Zero-Point Energy in High-Dimensional Molecular Systems

Sophya Garashchuk
University of South Carolina--Columbia, sgarashc@chem.sc.edu

Vitaly A. Rassolov
University of South Carolina - Columbia, rassolov@chem.sc.edu

Publication Info

Preprint version *Journal of Chemical Physics*, Volume 129, Issue 2, 2008, pages 024109-.

Stable long-time semiclassical description of zero-point energy in high-dimensional molecular systems

Sophya Garashchuk[a] and Vitaly A. Rassolov
Department of Chemistry and Biochemistry, University of South Carolina, South Carolina 29208, USA

(Received 18 April 2008; accepted 29 May 2008; published online 10 July 2008)

Semiclassical implementation of the quantum trajectory formalism [J. Chem. Phys. **120**, 1181 (2004)] is further developed to give a stable long-time description of zero-point energy in anharmonic systems of high dimensionality. The method is based on a numerically cheap linearized quantum force approach; stabilizing terms compensating for the linearization errors are added into the time-evolution equations for the classical and nonclassical components of the momentum operator. The wave function normalization and energy are rigorously conserved. Numerical tests are performed for model systems of up to 40 degrees of freedom. © *2008 American Institute of Physics*. [DOI: 10.1063/1.2949095]

I. INTRODUCTION

Classical molecular dynamics provides a reasonable general picture of chemical reaction dynamics in most systems of practical interest. However, the isotope effect measurements and comparison of typical reaction energies and zero-point energy (ZPE) show that quantum mechanical (QM) effects play an important role in many systems, particularly for reactions of proton transfer (some examples can be found in Refs. 1–3). The adequate theoretical description of quantum effects has been proven to be a very challenging task. The collective research over the past three decades points to three primary reasons: (i) many reactions occur at the time scale much longer than that of a typical quantum dynamics simulation, (ii) the forces acting on the reactive species are not well represented by simple harmonic approximations, and (iii) quantum effects such as ZPE require an ensemble rather than an individual trajectory description. Below we present a computational method that is easily compatible with multidimensional molecular mechanics, accounts for quantum effects in an approximate yet rigorous manner for an arbitrary long propagation time and, in principle, is improvable toward the full quantum limit.

The de Broglie–Bohm form of the time-dependent Schrödinger equation[4] is a trajectory-based formulation of quantum mechanics in terms of the real phase, $S(x,t)$, and amplitude, $A(x,t)$, of a wave function,

$$\psi(x,t) = A(x,t)\exp\left(\frac{\imath}{\hbar}S(x,t)\right), \tag{1}$$

given in this section for a particle of mass m in one dimension for simplicity. The prime symbol denotes differentiation with respect to x. The quantum trajectories are defined by their positions x and *classical* momenta p,

$$p(x,t) = S'(x,t), \tag{2}$$

evolving according to Hamilton's equations of motion,

$$\frac{dx}{dt} = \frac{p}{m}, \frac{dp}{dt} = -V' - U'. \tag{3}$$

The trajectory "weight" w, or probability associated with the volume element δx of a trajectory, remains constant in time for closed systems,[5]

$$w(x,t) = A^2(x,t)\,\delta x(t), \quad \frac{dw}{dt} = 0. \tag{4}$$

$S(x,t)$ is the classical action function

$$\frac{dS}{dt} = \frac{p^2}{2m} - (V+U). \tag{5}$$

All QM nonlocality is expressed in the quantum potential U acting on a trajectory in addition to the external, or classical, potential V,

$$U = -\frac{\hbar^2}{m}(r^2 + r'). \tag{6}$$

The quantity $r=r(x,t)$ is the *nonclassical* component of the momentum operator,

$$r(x,t) = \frac{A'(x,t)}{A(x,t)}. \tag{7}$$

The expectation value of the quantum potential can be termed "quantum energy"—the energy due to the shape of the wave function amplitude. Integration of Eq. (6) with differentiation by parts gives

$$\langle U\rangle = \frac{\hbar^2}{2m}\langle r^2\rangle, \tag{8}$$

so that the total energy can be written as

$$E = \frac{\langle p^2\rangle}{2m} + \langle V\rangle + \frac{\hbar^2\langle r^2\rangle}{2m}. \tag{9}$$

Throughout the paper, we use Dirac notations to define an average value of an operator multiplicative in the coordinate representation,

[a]Electronic mail: sgarashc@mail.chem.sc.edu.

$$\langle \hat{o}(x,t)\rangle = \int o(x(t))A^2(x,t)\delta x(t) \approx \sum_{i=1}^{N_{\text{traj}}} o(x_i(t))w_i. \quad (10)$$

The last equality in Eq. (10) is given for numerical implementation with the initial wave function discretized in terms of N_{traj} trajectories. Atomic units of $\hbar=1$ are used below.

While the quantum trajectory formulation gives a straightforward connection to classical mechanics—for a nonsingular wave function amplitude, the quantum potential U vanishes in the limit of $\hbar\to 0$ or $m\to\infty$—the exact numerical implementation of the formalism is, in general, challenging and expensive: U is singular at the nodes of the wave function and the dynamics of quantum trajectories is extremely sensitive to the accuracy of the quantum force near the nodes. (For a review of the quantum trajectory methods, the reader is referred to Ref. 6.) Therefore, we are developing a semiclassical implementation of the quantum trajectory formalism based on the approximate quantum potential (AQP).[5,7] In the AQP method, the nonclassical momentum is approximated globally as a linear combination of a small number N_{bas} of basis functions $\vec{f}=(f_1,f_2,\ldots)$,

$$\tilde{r}=\vec{c}\cdot\vec{f}\approx\frac{A'(x,t)}{A(x,t)}. \quad (11)$$

Then, AQP $\tilde{U}$,

$$\tilde{U}=-\frac{\tilde{r}^2+\tilde{r}'}{2m}, \quad (12)$$

and its gradient needed in Eq. (3) are obtained analytically. The optimal values of the expansion coefficients $\vec{c}$ used in Eq. (12) are the solutions of a linear minimization of a functional I with respect to the elements of $\vec{c}$,

$$I=\langle(\tilde{r}-A^{-1}A')^2\rangle, \quad \nabla_c I=0. \quad (13)$$

Differentiation by parts in Eqs. (13) and (4) enables one to express all required quantities in terms of the moments of the trajectory distribution. The resulting dynamics of an ensemble of trajectories is numerically stable and energy conserving. Scaling with respect to the number of trajectories is linear.[7] Note that so far, $r(x,t)$ was used as a definition, $r(x,t)\equiv A^{-1}A'$, *not* as an independent function.

Formally, the nonclassical momentum $r(x,t)$ can be computed along trajectories just as $p(x,t)$ is computed according to the time-evolution equations

$$\frac{dp}{dt}=-V'+\frac{1}{2m}\left(2r(x,t)\frac{d}{dx}+\frac{d^2}{dx^2}\right)r(x,t), \quad (14)$$

$$\frac{dr}{dt}=-\frac{1}{2m}\left(2r(x,t)\frac{d}{dx}+\frac{d^2}{dx^2}\right)p(x,t). \quad (15)$$

Differential operators in the equations above are identical, and straightforward computation of $r(x,t)$ would entail the same difficulties as encountered in the computation of the quantum force. Equations (14) and (15) are solved approximately in the derivative propagation method,[8] the Bohmian trajectory stability method,[9] and the Bohmian mechanics with complex action approach[10] as part of a truncated hierarchy of equations based on $\hbar$ expansions. In contrast, we do not expand Eqs. (14) and (15) but use the AQP-type approximation to find the derivatives of $r(x,t)$ and $p(x,t)$ to solve these equations. Then, $r(x,t)$ becomes a trajectory-specific variable on par with $p(x,t)$ and $S(x,t)$: Eq. (7) defines the initial values $r(x,0)$, but it will not be fulfilled at later times unless time evolution of $r(x,t)$ and $p(x,t)$ is exact. Function $r(x,t)$ obtained along trajectories can be compared to $\tilde{r}$ defined by Eqs. (11) and (13) and used to assess and correct the AQP error.

A particular form of AQP—the linearized quantum force[5] (LQF)—obtained by representing $\tilde{r}$ in a linear basis, is the simplest and the cheapest AQP method. It is exact for Gaussian wavepackets and, in general, is capable of describing leading quantum effects, such as the wavepacket bifurcation, moderate tunneling, and ZPE. LQF also fulfills an important property of the exact quantum force F_q,

$$\langle F_q\rangle=-\langle U'\rangle=0, \quad (16)$$

and is invariant under rotation of coordinates. It was found, however, that in semibound potentials, the quantum energy was described correctly only on a short time scale (half of the oscillation period): trajectories from the wavepacket fringes "evaporated" into the dissociation region, leading to quick loss of the quantum energy in the ensemble because in LQF, the average quantum potential is inversely proportional to the wave function dispersion $\sigma=\langle x^2\rangle-\langle x\rangle^2$. In bound anharmonic potentials, LQF trajectories "decohere" and lead to nonzero but significantly underestimate ZPE values. These issues can be resolved by defining LQF on subspaces or domains,[11] by using a more flexible or system-specific basis $\vec{f}$,[12,13] or by using a stabilizing friction force.[14] In general, the first two methods give exact QM dynamics in the limit of a large number of domains/basis functions, but in the regime of a few domains/basis functions, they improve the ZPE description on a finite time scale (several oscillation periods) and they are more expensive than LQF. The friction method stabilizes the dynamics with respect to small anharmonicity and reproduces ZPE for dozens of oscillation periods, but it has an adjustable "friction coefficient" and does not conserve the total energy.

In the remainder of the paper, we describe a new way of improving the ZPE description on an essentially infinite time scale using both $r(x,t)$ computed from Eq. (15) and linearization of $A^{-1}A'$. The method is energy and norm conserving, is parameter-free, and has numerical cost nearly as low as that of LQF. The theory is described in Sec. II in many dimensions. Wavepacket dynamics in one-dimensional anharmonic potentials typical of nuclear dynamics and scattering on the Eckart barrier in the presence of multiple Morse oscillators are described and discussed in Sec. III. Section IV concludes.

II. TIME-EVOLUTION WITH BALANCED ERRORS

A. Approximation of gradients

For a system described in N_{dim} Cartesian coordinates $(x,y,\ldots)$ using vector notations,

$$\vec{p} = \nabla S, \quad \vec{r} = A^{-1}\nabla A, \tag{17}$$

the time evolution of $\vec{r}$ and $\vec{p}$ given by Eqs. (14) and (15) is generalized as

$$m\left(\frac{d\vec{p}}{dt} + \nabla V\right) = (\vec{r}\cdot\nabla)\vec{r} + \frac{(\nabla\cdot\nabla)\vec{r}}{2} - m\frac{d\vec{r}}{dt}$$
$$= (\vec{r}\cdot\nabla)\vec{p} + \frac{(\nabla\cdot\nabla)\vec{p}}{2}. \tag{18}$$

For practical reasons, we use global approximations to $\vec{r}$ and $\vec{p}$ to estimate their derivatives on the right-hand side of Eq. (18). In the linear approximation to $\vec{r}$ and $\vec{p}$, the terms with the Laplacian operators become zeros. We define a minimization procedure similar to the LQF approach and require conservation of the total energy E given by Eq. (9), $dE/dt = 0$. This requirement couples fitting of $A^{-1}\nabla A$ and $\vec{p}$.

Let us use the linear basis $\vec{f} = (x, y, \ldots, 1)$ and arrange the fitting coefficients of the components of $A^{-1}\nabla A$ into a matrix $\mathbf{C}^r$,

$$\mathbf{C}^r = [\vec{c}_x^r, \vec{c}_y^r, \ldots], \tag{19}$$

where functions $\{\tilde{r}_x = \vec{c}_x^r\cdot\vec{f}, \tilde{r}_y = \vec{c}_y^r\cdot\vec{f}, \ldots\}$ approximate components of the vector $A^{-1}\nabla A$. Similarly, matrix $\mathbf{C}^p$ contains fitting coefficients for the components of classical momentum $\vec{p}$,

$$\mathbf{C}^p = [\vec{c}_x^p, \vec{c}_y^p, \ldots], \tag{20}$$

where functions $\{\tilde{p}_x = \vec{c}_x^p\cdot\vec{f}, \tilde{p}_y = \vec{c}_y^p\cdot\vec{f}, \ldots\}$ approximate components of the vector $\vec{p}$. For a system of dimensionality N_{dim}, the basis size is $N_{\mathrm{bas}} = N_{\mathrm{dim}} + 1$. Differentiating Eq. (9) with respect to time and using Eq. (18) with the derivatives obtained from the linear approximations to $A^{-1}\nabla A$ and $\vec{p}$, the energy conservation condition becomes

$$\frac{dE}{dt} = \frac{\langle\vec{r}^0\cdot(\mathbf{C}^r\vec{p} - \mathbf{C}^p\vec{r})\rangle}{m} = 0. \tag{21}$$

Quantity $\vec{r}^0$ denotes a vector of nonclassical momentum extended to the size of the basis

$$\vec{r}^0 = (r_x, r_y, \ldots, 0). \tag{22}$$

For a general basis, the energy conservation is expressed as

$$\langle\vec{r}(\mathbf{F}^r\vec{p} - \mathbf{F}^p\vec{r})\rangle = 0$$

in terms of matrices $\mathbf{F}^r$ and $\mathbf{F}^p$ with elements

$$F_{xy}^r = \langle\partial\tilde{r}_x/\partial y\rangle, \quad F_{xy}^p = \langle\partial\tilde{p}_x/\partial y\rangle \tag{23}$$

where indices x and y span all dimensions. If approximations are exact, then $\vec{r}$ and $\vec{p}$ satisfy Eq. (17) and $\mathbf{F}^r$ and $\mathbf{F}^p$ are symmetric matrices. This symmetry property is also fulfilled for the linear basis approximation, so that $\mathbf{C}^r$ and $\mathbf{C}^p$ are symmetric matrices.

The least squares fit of $A^{-1}\nabla A$ and $\vec{p}$ in terms of a linear basis with the constraint (21) included through the Lagrange multiplier 2λ, written as a minimization of a functional,

$$I = \langle\|A^{-1}\nabla A - \mathbf{C}^r\vec{f}\|^2\rangle + \langle\|\vec{p} - \mathbf{C}^p\vec{f}\|^2\rangle$$
$$+ 2\lambda\langle\vec{r}^0\cdot(\mathbf{C}^r\vec{p} - \mathbf{C}^p\vec{r})\rangle, \tag{24}$$

is solved by the system of linear equations,

$$\begin{pmatrix} \mathbf{M} & \mathbf{O} & \vec{\mathbf{D}}^p \\ \mathbf{O} & \mathbf{M} & \vec{\mathbf{D}}^r \\ \vec{\mathbf{D}}^p & \vec{\mathbf{D}}^r & 0 \end{pmatrix}\cdot\begin{pmatrix} \vec{\mathbf{C}}^r \\ \vec{\mathbf{C}}^p \\ \lambda \end{pmatrix} = \begin{pmatrix} \vec{\mathbf{B}}^r \\ \vec{\mathbf{B}}^p \\ 0 \end{pmatrix}. \tag{25}$$

In Eq. (25) the following matrices and vectors are introduced: (i) $\mathbf{M}$ is the block-diagonal matrix of dimensionality $N_{\mathrm{dim}}N_{\mathrm{bas}} \times N_{\mathrm{dim}}N_{\mathrm{bas}}$ with the basis function overlap matrix $\mathbf{S} = \langle\vec{f}\otimes\vec{f}\rangle$ as N_{dim} diagonal blocks; (ii) $\mathbf{O}$ is a zero matrix of the same size as $\mathbf{M}$; (iii) the elements of the vectors $\vec{\mathbf{C}}^r$, $\vec{\mathbf{C}}^p$, $\vec{\mathbf{B}}^r$, $\vec{\mathbf{B}}^p$, $\vec{\mathbf{D}}^r$, and $\vec{\mathbf{D}}^p$ are the elements of the matrices $\mathbf{C}^r$, $\mathbf{C}^p$, $\mathbf{B}^r$, $\mathbf{B}^p$, $\mathbf{D}^r$, and $\mathbf{D}^p$, respectively, listed in a column after column order. $\mathbf{C}^r$ and $\mathbf{C}^p$ are given by Eqs. (19) and (20). The remaining four matrices are defined as

$$\mathbf{B}^r = -\frac{1}{2}\langle(\nabla\otimes\vec{f})^T\rangle, \quad \mathbf{B}^p = \langle\vec{f}\otimes\vec{p}\rangle, \tag{26}$$

$$\mathbf{D}^r = -\langle\vec{r}^0\otimes\vec{r}\rangle, \quad \mathbf{D}^p = \langle\vec{p}^0\otimes\vec{r}\rangle, \tag{27}$$

where $\vec{p}^0$ denotes a vector of classical momentum extended to the size of the basis,

$$\vec{p}^0 = (p_x, p_y, \ldots, 0). \tag{28}$$

Fitting of $A^{-1}\nabla A$ is the same as in the LQF procedure, except that now it is coupled to the least squares fit of $\vec{p}$. Formally, the total size of the matrix in Eq. (25) is $2N_{\mathrm{dim}}N_{\mathrm{bas}} + 1$, but its structure allows one to solve Eq. (25) by performing a single matrix inversion of block $\mathbf{S}$ of size N_{bas},[15] so that the cost of the quantum force computation scales as $N_{\mathrm{traj}}N_{\mathrm{dim}}^2$. This is essential for efficient high-dimensional implementation.

Conceptually, this approximation scheme has the following desirable features: (i) the total energy of the wavepacket defined by Eq. (9) is conserved; (ii) the approximate quantum force vanishes for delocalized wave functions; (iii) the AQP parameters explicitly depend on trajectory positions *and* momenta improving the quality of approximation. In the linear approximation of $\vec{r}$ and $\vec{p}$, the Laplacian term in Eq. (18) is zero. Consequently, in an anharmonic system, $\vec{r}$ can become quite different from $A^{-1}\nabla A$ defined by the trajectory positions and the wave function probability conservation property given by Eq. (4). This problem is addressed below.

B. Correction of linearization effect on dynamics

While the numerically cheap linear basis $\vec{f}$ describes exact dynamics in the important limit of Gaussian wave functions evolving in locally harmonic potentials, in most practical applications, the ZPE description should be stable to small deviations from the Gaussian shape of wave functions, i.e., stable to small nonlinearity of $\vec{p}$ and $\vec{r}$. Therefore, in Eq. (18) instead of the Laplacian terms which are zero in the linear basis representation, we introduce additional terms dependent on the difference of exact and approximated values

of $\vec{p}$ and $\vec{r}$. These extra terms balance errors associated with the linear basis in the first order of the nonlinearity parameters. The explicit form is determined from the analytical models and has no adjustable parameters.

We consider quadratic momentum and the lowest order nonlinearity in r,

$$p = p_0 + p_1 x + \epsilon x^2, \quad |\psi|^2 = \exp(-\alpha x^2)(1 + \delta(x - x_0))^2. \tag{29}$$

Determining the linear approximations to p from minimization of $\langle (p-\tilde{p})^2 \rangle$ and to r from minimization of $\langle (r-\tilde{r})^2 \rangle$, it was found that the following approximate equations of motion:

$$m\left(\frac{dp}{dt} + V'\right) = rr' + \frac{r''}{2} = r\tilde{r}' + 2\tilde{r}'(r-\tilde{r}) + O(\delta^4) - m\frac{dr}{dt}$$
$$= rp' + \frac{p''}{2} = r\tilde{p}' + 2\tilde{r}'(p-\tilde{p}) + O(\epsilon\delta^3), \tag{30}$$

cancel the leading errors in δ and ϵ.

In the multidimensional case, derivatives $\tilde{r}'$ and $\tilde{p}'$ of the approximate functions generalize into matrices $\mathbf{F}^r$ and $\mathbf{F}^p$ given by Eq. (23), and the approximate time-evolution equations become

$$-m\frac{d\vec{r}}{dt} = \mathbf{F}^p\vec{r} + 2\mathbf{F}^r(\vec{p} - \vec{p}^{\,\mathrm{fit}}),$$
$$m\left(\frac{\vec{p}}{dt} + \nabla V\right) = \mathbf{F}^r\vec{r} + 2\mathbf{F}^r(\vec{r} - \vec{r}^{\,\mathrm{fit}}). \tag{31}$$

In Sec. II A, functions $\{\tilde{r}_x, \tilde{r}_y, \ldots\}$ approximate components of $A^{-1}\nabla A$ and their determination is coupled to approximation of $\vec{p}$ in terms of $\{\tilde{p}_x, \tilde{p}_y, \ldots\}$ by the energy conservation condition. In contrast, $\vec{r}^{\,\mathrm{fit}}$ approximates $\vec{r}$ and, in general, components of $\vec{r}^{\,\mathrm{fit}}$ can be different from the corresponding functions $\tilde{r}_i$. We require that the stabilization terms do not contribute to the total energy of the ensemble and that the property $\langle d\vec{r}/dt \rangle = 0$ derived from the wave function norm conservation, $\langle \psi(t) | \psi(t) \rangle = 1$, is fulfilled. In principle, a minimization procedure for $\langle \|\vec{r} - \vec{r}^{\,\mathrm{fit}}\|^2 \rangle$ coupled to minimization of $\langle \|\vec{p}^{\,\mathrm{fit}} - \vec{p}\|^2 \rangle$ by the above mentioned requirements can be established similar to Sec. II A. However, in the case of the linear basis, these requirements are met if $\vec{r}^{\,\mathrm{fit}}$ and $\vec{p}^{\,\mathrm{fit}}$ are found from the standard least squares fits of $\vec{r}$ and $\vec{p}$. These fits require minimal additional computation efforts because the solution involves the same basis function overlap matrix $\mathbf{S}$ as in Sec. II A.

III. NUMERICAL EXAMPLES

A. Dynamics in one dimension

Numerical tests were performed for anharmonic one-dimensional systems described in Refs. 11 and 14. As a preliminary check, we have verified that introduction of the stabilization terms do not affect bifurcation of a wavepacket scattering on the Eckart barrier. In order to analyze the effects of linearization and stabilization terms in time evolution equations (14) and (15), here we consider the one-dimensional Morse oscillator in detail. The system represents a nonrotating hydrogen molecule and is described in atomic units scaled by the reduced mass of H_2, so that $m=1$. The initial wavepacket is a Gaussian wave function similar to the ground state of H_2, as described in Ref. 11.

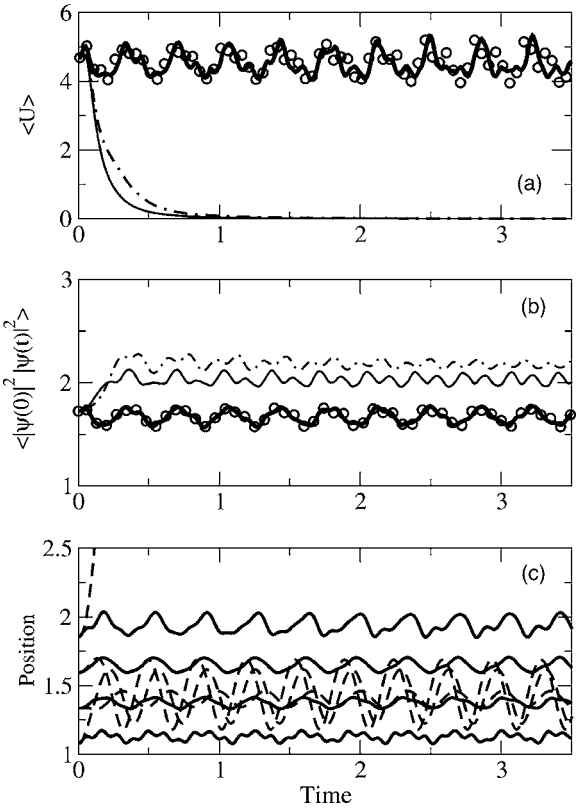

FIG. 1. Dynamics of the Morse oscillator. (a) The average quantum potential as a function of time obtained using LQF and the AQP with balanced errors method without and with the stabilization terms is shown with the thin solid line, dot-dashed line, and circles, respectively. The exact QM result is shown with the thick solid line. (b) The wave function density overlap, $\langle |\psi(0)|^2 |\psi(t)|^2 \rangle$, as a function of time. Legend is the same as in (a). (c) Trajectory positions as functions of time obtained using the LQF (dashed line) and the AQP with balanced errors method (solid line).

Figure 1(a) shows the expectation values of the quantum potential, $\langle U \rangle$, which is the quantum part of ZPE, obtained with the QM split operator method[16] and with the trajectory calculations using LQF and the new method with and without the stabilization term. In trajectory calculations, $\langle U \rangle$ is computed as an average of Eq. (12) for LQF and according to Eq. (8) otherwise. The LQF result shows decrease in $\langle U \rangle$ due to effect of linearization on dynamics detailed below. The same behavior is observed for the new method in the absence of stabilization terms. Once these terms are introduced, we have a stable ZPE description for many oscillation periods.

Figure 1(b) shows the overlap of the time-dependent wave function density with the initial density, $C(t) = \langle |\psi(0)|^2 |\psi(t)|^2 \rangle$. In the case of LQF and of the new method without stabilization terms, high energy trajectories on the fringes of the wavepacket leave the bound region of the potential by the following mechanism. In general, quantum force tends to delocalize the wave function: a wave function

in free space spreads indefinitely, while inside a well, the interplay between the parabolic barrierlike quantum potential and the confining classical potential results in the oscillations of the wavepacket width.

For the given system at short times, LQF, which is proportional to the displacement of a trajectory from the average position of the ensemble, is larger in magnitude than the counteracting classical force and, thus, the net force quickly pushes the fringe trajectories into the dissociation region. LQF is inversely proportional to the square of the wave function dispersion; therefore, the quantum force vanishes once trajectories leave the bound region. The dynamics of the trajectories becomes purely classical and bound trajectories oscillate independently of each other, i.e., the wavepacket decoheres, even if a small fraction of the wavepacket leaves the bound region. A similar behavior is observed when we define the quantum force in terms of computing along the trajectories $r(x,t)$ without the stabilization term because the quantum force proportional to C^r vanishes as dispersion grows, just as in the LQF dynamics. The stabilization term provides a correction to the dynamics if linearization of $r(x,t)$ deviates from the function itself, maintaining coherence between the approximate quantum trajectories.

Positions of the trajectories as functions of time are shown in Fig. 1(c). The minimum of the well is located at $x_m=1.4a_0$. Note the dissociating LQF trajectory. The trajectory stabilization is clearly manifested in small oscillations in the position of the lowest trajectory originated on the repulsive wall of the potential. With the stabilization mechanism implemented, the average quantum energy and the wave function density overlaps are in good agreement with the QM results. The trajectory propagation was accomplished with the third order Milne predictor-corrector algorithm[15] and the stability of the ZPE description was checked for up to 200 oscillation periods.

Application to dynamics in the parabolic well with quartic anharmonicity of Ref. 14 gave the same level of the ZPE description as for the Morse oscillator. An efficient description of the tunneling dynamics in a double well, which involves "hard" QM effects such as deep tunneling, interference, and wavepacket revivals on a long time scale, presents a major challenge to semiclassical methods and remains an outstanding challenge for the AQP method. A combination of stabilization approach and subspace description[11] may provide a solution.

B. Multidimensional systems

Application of approximate methods to high-dimensional systems has to be validated by tests that can be compared to exact QM results, which generally means separable Hamiltonians or harmonic potentials. For multidimensional testing of the AQP method whose accuracy, in principle, depends on the choice of coordinates or basis functions (with the exception of the linear expansion basis $\vec{f}$), we use a model potential consisting of the Eckart barrier in the reaction degree of freedom (centered at zero) and of the Morse oscillators in the vibrational degrees of freedom. Parameters of these one-dimensional potentials mimicking the $H+H_2$ system are given in Ref. 11. The initial multidimensional wavepacket is defined as a direct product of a Gaussian,

$$\psi(x,0) = (2\gamma\pi^{-1})^{1/4} \exp(-\gamma(x-x_0)^2 + \imath p_0(x-x_0)),$$

with parameter values $\{\gamma=6, x_0=4, p_0=6\}$ in the reaction degree of freedom and of Gaussians with the parameters $\{\gamma=9.33, x_0=x_m, p_0=0\}$ centered at the minimum of the well in the vibrational degrees of freedom.

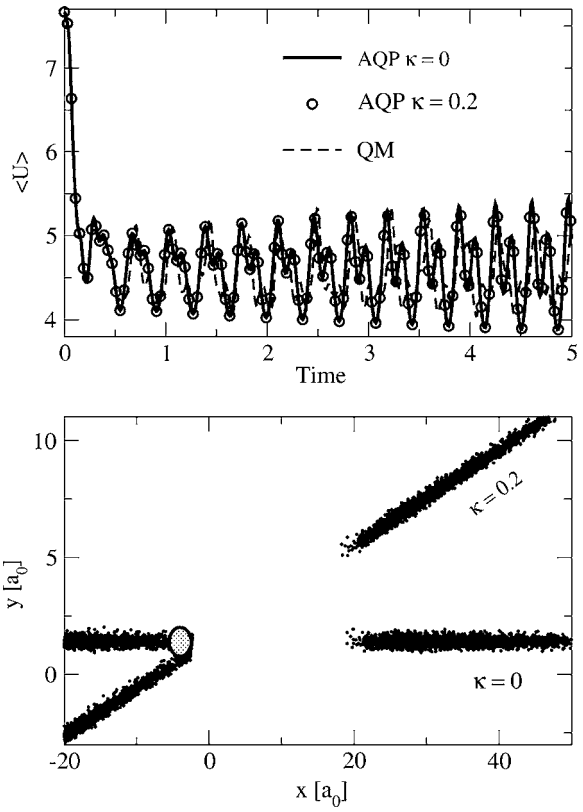

FIG. 2. Rotation in two dimensions. The upper panel shows the average quantum potential for $N_{\mathrm{dim}}=2$ with ($\kappa=0.2$) and without ($\kappa=0$) rotation as well as the long-time QM value of $\langle U\rangle$. The lower panel shows positions of trajectories after 14 oscillation periods for $\kappa=0$ (aligned horizontally) and $\kappa=0.2$ (aligned diagonally) calculations. Initial trajectory positions for $\kappa=0$ localized around $\{x=-4, y=1.4\}$ are indicated with an ellipse.

In order to introduce effective coupling between degrees of freedom, the dynamics is performed in the rotated system of coordinates where both the wavepacket and the classical potential are nonseparable. The numerical procedure of the quantum force computation and trajectory propagation uses no information about the separability of the original Hamiltonian. The rotation matrix specified by the parameter κ, written here for clarity for a four-dimensional system, is

$$\Omega = \begin{pmatrix} \alpha & -\kappa & -\kappa & -\kappa \\ \kappa & 1+\beta & \beta & \beta \\ \kappa & \beta & 1+\beta & \beta \\ \kappa & \beta & \beta & 1+\beta \end{pmatrix}, \tag{32}$$

with $\alpha=\sqrt{1-(N_{\mathrm{dim}}-1)\kappa^2}$ and $\beta=(\alpha-1)/(N_{\mathrm{dim}}-1)$. This transformation does not change the diagonal kinetic energy operator provided that masses for all dimensions are equal.

The new formalism is *invariant* under such transformation, as can be seen in Fig. 2. The top panel shows the aver-

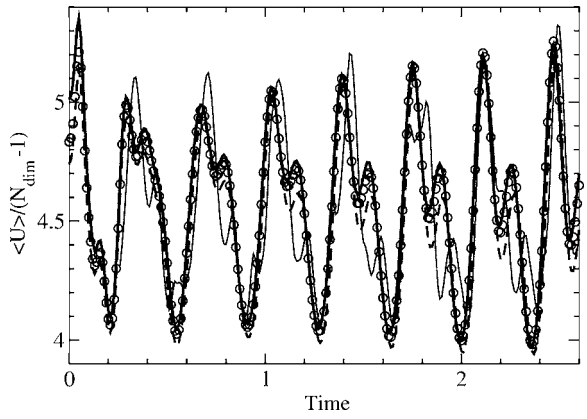

FIG. 3. Average quantum potential per vibrational degree of freedom for a Gaussian wavepacket scattering on the Eckart barrier in the presence of $N_{\mathrm{dim}}-1$ Morse oscillators. Semiclassical results are shown for $N_{\mathrm{dim}}=\{10,20,40\}$ with the thick solid line, circles, and dashed line, respectively. The QM result for long times is shown with a thin solid line.

age quantum potential for a two-dimensional system with and without rotation and the long-time exact QM result. The initial decrease in $\langle U\rangle$ for a two-dimensional system corresponds to the delocalization of the wavepacket in the reaction coordinate: the average quantum potential per vibrational degree of freedom is reduced to the average quantum potential of a one-dimensional Morse oscillator on the time scale of one vibrational period after the wavepacket bifurcates and delocalizes in the reaction degree of freedom. The bottom panel shows distribution of the quantum trajectories after 14 vibrational periods to illustrate the effect of the rotation of the system of coordinates. The initial position of the wavepacket for $\kappa=0$ is also indicated.

Numerical performance of the new method has been tested up to 40 dimensions with random Gaussian sampling of initial positions.[15] Calculation of the quantum potential and force is dominated by the computation of the moments of the trajectory distribution which scales as $N_{\mathrm{traj}}N_{\mathrm{dim}}^2$. Calculation of the global linearization parameters is performed at each time step for the ensemble of trajectories with the cost of N_{dim}^4. The average quantum potential divided by the number of the vibrational degrees of freedom, $\langle U\rangle/(N_{\mathrm{dim}}-1)$, is shown in Fig. 3. Semiclassical results reflect changes in the degree of wavepacket localization and their accuracy is essentially independent of the dimensionality. Convergence of the semiclassical results with respect to the number of trajectories is summarized in Table I for systems with 10, 20, and 40 degrees of freedom for calculations using 5×10^3, 10^4, and 2×10^4 trajectories. The relative average difference $\Delta=\langle U-U^{\mathrm{ex}}\rangle/\langle U^{\mathrm{ex}}\rangle$ and the standard deviations σ are shown. $\langle U^{\mathrm{ex}}\rangle$ is defined by the calculation with 4×10^4 trajectories. Calculations with 2×10^4 trajectories gave the relative difference of the quantum energy around 0.5% with the standard deviations of about 1% for all numbers of vibrational degrees of freedom. Pseudorandom sampling[15] or other sampling techniques of Monte Carlo integration can be used to improve convergence with respect to the number of trajectories. The largest calculation takes a few hours on a single processor of a dual-processor desktop workstation.

IV. CONCLUSIONS

In the quantum, or Bohmian, trajectory formulation of the time-dependent Schrödinger equation, the nonlocal nature of quantum mechanics is expressed in a single nonlocal quantity, the quantum potential, incorporated into an otherwise classical representation of motion for an ensemble of trajectories. For reasons of practicality, the quantum potential is determined approximately, yielding a semiclassical description of QM effects. In the cheapest implementation of this strategy—LQF—the quantum potential obtained from linearization of $A^{-1}\nabla A$ gives the *linear* quantum force and, thus an unphysical loss of ZPE in anharmonic systems on a short time scale. In this work we presented a novel way of doing quantum trajectory dynamics—AQP with balanced errors—where in addition to trajectory positions $\vec{x}$ and classical momenta $\vec{p}$, the nonclassical components of the momentum operator $\vec{r}$ are computed along the trajectories. Now the quantum force explicitly depends on a trajectory-specific $\vec{r}$ and, therefore is no longer restricted to the linear form.

A stable long-time description of QM effects requires that the positions of individual trajectories remain correlated because nonlocal information, by definition, depends on the relative quantities of the trajectory ensemble. In LQF this nonlocal information is derived from the moments of the trajectory distribution, so the QM effects are described as long as the trajectory distribution remains localized and coherent. In the new method, the quantum force depends on a trajectory-specific $\vec{r}$ and therefore, it is necessary to ensure that values of $\vec{r}$ remain correlated across the trajectory ensemble. This has been achieved by introducing stabilization terms into the time-evolution equations for $\vec{r}$ and $\vec{p}$.

Another aspect worth emphasizing is the use of the ensemble of trajectories in contrast to the methods based on the formal derivative expansion procedures centered on *indepen-*

TABLE I. Accuracy of the average quantum potential $\langle U\rangle$ over 15 oscillation periods for 10-, 20-, and 40-dimensional systems. The number of trajectories is given in the top row. Δ is the relative average difference and σ is the standard deviation for $\langle U\rangle$ obtained with $N_{\mathrm{traj}}\leq 2\times10^4$ trajectories compared to the $N_{\mathrm{traj}}=4\times10^4$ calculation.

N_{dim}		Δ (%)			σ (%)		$\langle U\rangle$
N_{traj}	5×10^3	1×10^4	2×10^4	5×10^3	1×10^4	2×10^4	4×10^4
10	1.68	0.84	0.52	2.16	1.21	0.62	41.44
20	2.07	1.09	0.40	2.92	1.59	1.09	87.07
40	⋯	0.89	0.32	⋯	2.58	1.22	177.5

dent trajectories, such as the derivative propagation method,[8] Bohmian trajectory stability approach,[9] and Bohmian mechanics with complex action.[10] The common feature of these independent trajectory methods is that all nonlocality comes from the derivatives of the wave function phase and amplitude computed along each trajectory. While propagation of independent trajectories implemented in parallel is appealing, we believe that it is very difficult, if not impossible, to obtain a stable long-time description of QM effects in anharmonic potentials with independent trajectories. In real system applications, numerical cost is dominated by computation of classical potential and forces; therefore, the numerical cost of the AQP computation and propagation of the trajectory ensemble rather than a set of independent trajectories is negligible.

To summarize, in the AQP with balanced errors approach, the time-evolution equations are solved approximately by defining gradients of the classical and nonclassical momenta from linearization of $\vec{p}$ and $A^{-1}\nabla A$. The effects of the linear approximation are compensated by the additional terms in the equations of motion determined from the analytical model of nonlinear $\vec{r}$ and $\vec{p}$. The linearization procedure is defined in such a way that the total energy of the system is conserved, and conditions on the total quantum force and wave function normalization are fulfilled. In the implementation with the linear basis, the method is invariant with respect to a unitary transformation of coordinates. The method is exact for correlated Gaussian wavepackets in locally harmonic potentials and describes ZPE in high-dimensional bound systems with small anharmonicity on the time scale of hundreds of oscillation periods in a numerically efficient way. We believe that propagation will be robust on an arbitrary long time scale with a more stable propagator than the one used in this work. The method has been implemented with random sampling, something that can be readily made more efficient with pseudorandom sampling or other advanced sampling techniques. The method may also be combined with larger basis sets and description on subspaces which will enable us to treat more general potentials, such as the double well coupled to anharmonic bath modes—the prototype system for simulation of quantum effects in condense environments.

ACKNOWLEDGMENTS

This material is based upon work supported by the National Science Foundation under Grant No. CHE-0516889.

[1] M. J. Knapp, K. Rickert, and J. P. Klinman, J. Am. Chem. Soc. **124**, 3865 (2002).
[2] B. R. Ussing, C. Hang, and D. A. Singleton, J. Am. Chem. Soc. **128**, 7594 (2006).
[3] S. Hammes-Schiffer, Acc. Chem. Res. **39**, 93 (2006).
[4] D. Bohm, Phys. Rev. **85**, 166 (1952).
[5] S. Garashchuk and V. A. Rassolov, J. Chem. Phys. **118**, 2482 (2003).
[6] R. E. Wyatt, *Quantum Dynamics with Trajectories: An Introduction to Quantum Hydrodynamics* (Springer-Verlag, Berlin, 2005).
[7] S. Garashchuk and V. A. Rassolov, J. Chem. Phys. **120**, 1181 (2004).
[8] C. J. Trahan, K. Hughes, and R. E. Wyatt, J. Chem. Phys. **118**, 9911 (2003).
[9] J. Liu and N. Makri, J. Phys. Chem. A **108**, 5408 (2004).
[10] Y. Goldfarb, I. Degani, and D. J. Tannor, J. Chem. Phys. **125**, 231103 (2006).
[11] V. A. Rassolov and S. Garashchuk, J. Chem. Phys. **120**, 6815 (2004).
[12] S. Garashchuk, V. A. Rassolov, and G. C. Schatz, J. Chem. Phys. **124**, 244307 (2006).
[13] S. Garashchuk and V. A. Rassolov, Chem. Phys. Lett. **446**, 395 (2007).
[14] S. Garashchuk and V. A. Rassolov, J. Phys. Chem. A **111**, 10251 (2007).
[15] W. Press, B. Flannery, S. Teukolsky, and W. Vetterling, *Numerical Recipes: The Art of Scientific Computing*, 2nd ed. (Cambridge University Press, Cambridge, 1992).
[16] M. D. Feit, J. A. Fleck, and A. Steiger, J. Comput. Phys. **47**, 412 (1982).